///VSP///

Advanced Composite Materials 18 (2009) 21–42

ADVANCED COMPOSITE MATERIALS
www.brill.nl/acm

Vibration and Post-buckling Behavior of Laminated Composite Doubly Curved Shell Structures

Chinmay Kumar Kundu and Jae-Hung Han *

Department of Aerospace Engineering, Korea Advanced Institute of Science and Technology, 335 Gwahangno (373-1 Guseong dong), Yuseong-gu, Daejeon 305-701, Korea

Received 8 November 2007; accepted 19 January 2008

Abstract

The vibration characteristics of post-buckled laminated composite doubly curved shells are investigated. The finite element method is used for the analysis of post-buckling and free vibration of post-buckled laminated shells. The geometric non-linear finite element model includes the general non-linear terms in the strain–displacement relationships. The shell geometry used in the present formulation is derived using an orthogonal curvilinear coordinate system. Based on the principle of virtual work the non-linear finite element equations are derived. Arc-length method is implemented to capture the load–displacement equilibrium curve. The vibration characteristics of post-buckled shell are performed using tangent stiffness obtained from the converged deflection. The code is first validated and then employed to generate numerical results. Parametric studies are performed to analyze the snapping and vibration characteristics. The relationship between loads and fundamental frequencies and between loads and the corresponding displacements are determined for various parameters such as thickness ratio and shallowness.

Keywords

Vibration, snapping, finite element method, composite shells, curvilinear coordinates

1. Introduction

In order to achieve the desired structural design requirements, various laminated composite shell components are increasingly used in aircrafts, space vehicles and automotive structures. The aerospace organizations are intensively involved in the development of advanced composite materials for design, analysis and manufacturing structures in order to reduce the weight and cost while increasing the lifetime and operational performance. During their service life, those composite shell struc-

* To whom correspondence should be addressed. E-mail: jaehunghan@kaist.ac.kr
Edited by KSCM

 DOI:10.1163/156855108X385320

tures may experience large bending deformation resulting in pre-buckling and post-buckling due to higher external loading and the shells may exhibit snap-through and snap-back type post-buckling behavior. Under compressive loading the shell panels have unstable buckling characteristics, called snap-through and snap-back phenomena. During the snapping phenomenon the dynamic instability may be induced. The vibratory characteristics of post-buckled structures are a problem of primary importance in many engineering fields, including aerospace applications. It is well known that the buckling does not mean the ultimate failure of structures. The laminated plate is still capable of carrying some amount of load without failure after the buckling point. Particularly, the behavior of doubly curved composite shell panel is very complicated due to their geometric complexity, high anisotropy, loading and boundary conditions. However, lighter and more efficient structures can be manufactured to withstand higher design load. Therefore, it is necessary to investigate the post-buckling and snapping behavior of doubly curved shells under higher mechanical loads. Due to availability of high speed computers, accuracy rather then simplicity plays a vital rule for design and analysis of complex problems. For the analysis of geometric non-linear problems, the selection of the strain–displacement relationship is important. Therefore, in the present study, the strain–displacement relations employed for the vibration characteristics of pre-/post-buckled composite shell problems are derived from the three-dimensional theory of elasticity and the equilibrium equations are generally established using the virtual work principle for numerical analysis.

Geometric non-linear finite element formulation for the analysis for plates and shells has been presented by many researchers and scientists. For example, Wood and Zienkiewicz [1] investigated the non-linear analysis of beams, frames and arches, in a total Lagrangian co-ordinate system. The non-linear equilibrium equations are solved using the Newton–Raphson method. Bathe *et al.* [2] formulated a finite element method for static and dynamic analysis of structures undergoing large deformation. The formulation was derived from general principle of continuum mechanics. A Rayleigh–Ritz approach for the determination of the static deflection, in-plane stress distribution and natural frequencies of vibration of simply supported, rectangular plates subject to uni-axial in-plane loads was presented by Ilanko and Dickinson [3]. An analytical study was conducted by Palazotto and Linnemann [4] to determine the fundamental frequencies and critical buckling loads for laminated anisotropic circular cylindrical shell panels by using the Galerkin technique. An analytic method was studied for post-buckling and mode jumping behavior of bi-axially compressed composite laminates plate subjecting to bi-axially compression by Souza [5]. Lee and Lee [6] investigated the post-buckling and vibration behaviour of thermally buckled anisotropic plates subjected to uniform temperature change using the von Karman strain–displacement relation and solved the equilibrium equations using the Newton–Raphson method. Non-linear finite element equations based on the layerwise displacement theory was investigated by Oh *et al.* [7] for thermopiezoelastic analysis of laminated plates. Chen and Yu [8]

presented a mathematically rigorous approach to investigate the post-buckling response and mode jumping of simply-supported laminated composite plates. Teng and Hong [9] addressed the importance of strain–displacement relations, derived directly from the three-dimensional theory of elasticity. They presented a complete set of non-linear strain–displacement relations for shells in the sense that no term has been neglected based on the judgment of its relative magnitude. Later, the post-buckling analysis of laminated composite spherical, cylindrical and conoidal shells, considering the strain–displacement relations in the curvilinear coordinate system was presented by Kundu and Sinha [10]. Jha and Inman [11] discussed the importance of geometric non-linearity [9] for analysis of gossamer structures, considering membrane effects. Crisfield [12] presented arc-length method for the solution of non-linear problems.

It is observed from the open literature that limited work has been reported on vibratory characteristics of post-buckled laminated doubly shells. The present investigation focuses on the vibration characteristics of pre-buckled and post-buckled laminated composite spherical and cylindrical shells using the finite element method. The general geometrically non-linear strain–displacement relations are derived from the three-dimensional elastic body in the orthogonal curvilinear coordinate system. So a geometrically non-linear nine noded isoparametric doubly curved laminated shell element is developed. The mathematical formulation is based on the virtual work equations for a continuum with a total Lagrangian approach, and the material behavior is assumed to be linear and elastic. The non-linear equations are solved by the arc-length method and it can handle snap-through and snap-back behavior. A finite element code in C++ language is written to implement the above finite element formulation. Parametric studies are carried out for various thickness ratio and shallowness for laminated spherical and cylindrical shell panels. The effect of number of layers (n) in $[0/90]_n$ laminated shells on vibration behavior of post-buckled spherical shell is presented.

2. Finite Element Formulation

The shell geometry used in the present formulation is derived using an orthogonal curvilinear coordinate system [13], α_1 and α_2 along the lines of principal curvatures, and a normal coordinate ζ. The middle surface of the doubly curved laminated shell is assumed to be the reference surface and is shown in Fig. 1. The mid-surface which defines the shape of a shell is described by the two Lamε parameters, A_1 and A_2, and the two principal radii of the curvatures, R_1 and R_2. Consider a general thin laminate of thickness h composed of arbitrary oriented layers as shown in Fig. 1, with each lamina having different thickness as well as arbitrary fiber orientation θ with respect to the α_1 axis of the coordinate system as shown in Fig. 2 and laminate configuration shown in Fig. 3.

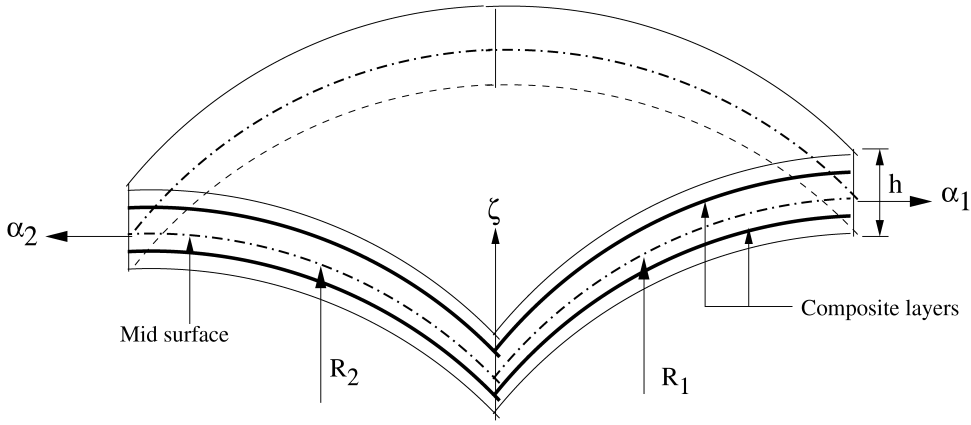

Figure 1. Geometry of a laminated doubly curved shell.

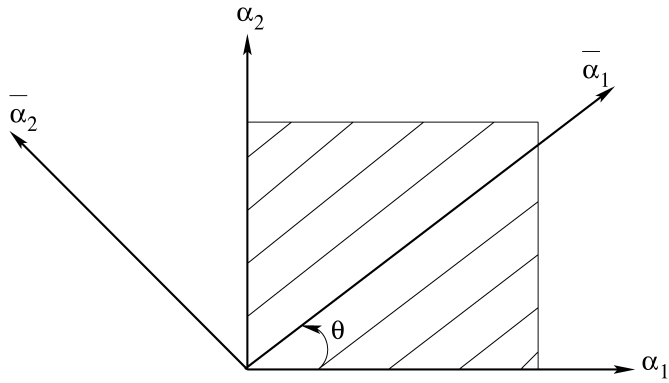

Figure 2. Laminate configuration.

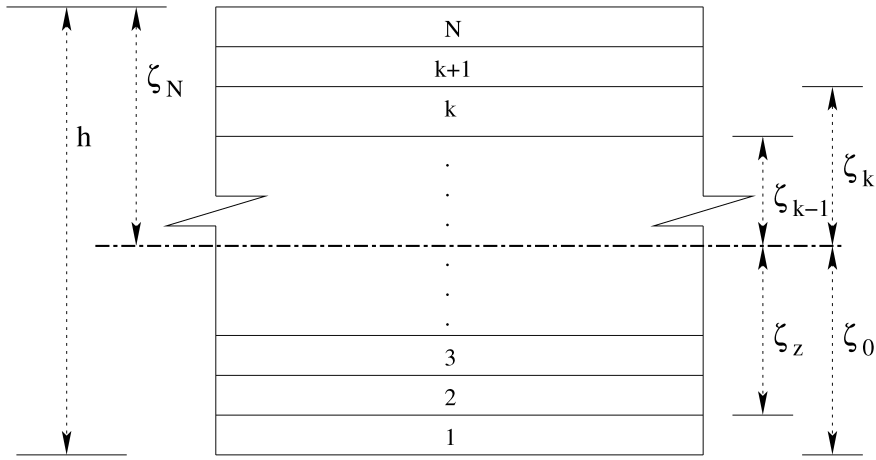

Figure 3. Layer details in a laminate.

2.1. Displacement Model

The displacements at any point can be described as:

$$\begin{aligned} u_1(\alpha_1,\alpha_2,\zeta) &= u_1^0(\alpha_1,\alpha_2) + \zeta\theta_1(\alpha_1,\alpha_2),\\ u_2(\alpha_1,\alpha_2,\zeta) &= u_2^0(\alpha_1,\alpha_2) + \zeta\theta_2(\alpha_1,\alpha_2),\\ w(\alpha_1,\alpha_2,\zeta) &= w^0(\alpha_1,\alpha_2), \end{aligned} \tag{1}$$

where u_1^0, u_2^0 and w^0 are the displacements on the reference surface along the α_1, α_2 and ζ directions, respectively; θ_1 and θ_2 are the rotations along the α_1 and α_2 directions, respectively.

2.2. Strain–Displacement Relations

The non-linear strain–displacement relations are derived from any three-dimensional elastic body [14], in an orthogonal curvilinear coordinate system and the first-order shear deformation theory is considered. The strain–displacement relations are derived in [10] and are expressed as follows:

$$\begin{aligned} \varepsilon_{11} &= \varepsilon_1^0 + \frac{1}{2}\left[(\varepsilon_1^0)^2 + (\varepsilon_3^0)^2 + (\varepsilon_5^0)^2\right] + \zeta\kappa_1,\\ \varepsilon_{22} &= \varepsilon_2^0 + \frac{1}{2}\left[(\varepsilon_2^0)^2 + (\varepsilon_4^0)^2 + (\varepsilon_6^0)^2\right] + \zeta\kappa_2,\\ \gamma_{12} &= (\varepsilon_3^0 + \varepsilon_4^0) + (\varepsilon_1^0\varepsilon_4^0 + \varepsilon_2^0\varepsilon_3^0 + \varepsilon_5^0\varepsilon_6^0) + \zeta(\kappa_3 + \kappa_4),\\ \gamma_{13} &= \varepsilon_5^0 + \theta_1,\\ \gamma_{23} &= \varepsilon_6^0 + \theta_2. \end{aligned} \tag{2}$$

The strain components ε in equation (2) can be separated into two parts, ε_l^0 and ε_{nl}^0,

$$\{\varepsilon^0\} = \{\varepsilon_l^0\} + \{\varepsilon_{nl}^0\} = \left([B_l] + \frac{1}{2}[B_{nl}]\right)\{\delta\}, \tag{3}$$

where $[B_l]$ and $[B_{nl}]$ are the linear and non-linear strain matrices; and $\{\delta\}$ is the element nodal displacement vector. The mid-surface strains and curvature terms are explicitly expressed as follows:

$$\begin{aligned} \varepsilon_1^0 &= \frac{1}{A_1}\frac{\partial u_1^0}{\partial\alpha_1} + \frac{u_2^0}{A_1A_2}\frac{\partial A_1}{\partial\alpha_2} + \frac{w^0}{R_1},\\ \varepsilon_2^0 &= \frac{1}{A_2}\frac{\partial u_2^0}{\partial\alpha_2} + \frac{u_1^0}{A_1A_2}\frac{\partial A_2}{\partial\alpha_1} + \frac{w^0}{R_2},\\ \varepsilon_3^0 &= \frac{1}{A_1}\frac{\partial u_2^0}{\partial\alpha_1} - \frac{u_1^0}{A_1A_2}\frac{\partial A_1}{\partial\alpha_2}, \qquad \varepsilon_4^0 = \frac{1}{A_2}\frac{\partial u_1^0}{\partial\alpha_2} - \frac{u_2^0}{A_1A_2}\frac{\partial A_2}{\partial\alpha_1},\\ \varepsilon_5^0 &= \frac{1}{A_1}\frac{\partial w^0}{\partial\alpha_1} - \frac{u_1^0}{R_1}, \qquad \varepsilon_6^0 = \frac{1}{A_2}\frac{\partial w^0}{\partial\alpha_2} - \frac{u_2^0}{R_2}, \end{aligned} \tag{4}$$

$$\kappa_1 = \frac{1}{A_1}\frac{\partial \theta_1}{\partial \alpha_1} + \frac{\theta_2}{A_1 A_2}\frac{\partial A_1}{\partial \alpha_2}, \qquad \kappa_2 = \frac{1}{A_2}\frac{\partial \theta_2}{\partial \alpha_2} + \frac{\theta_1}{A_1 A_2}\frac{\partial A_2}{\partial \alpha_1},$$
$$\kappa_3 = \frac{1}{A_1}\frac{\partial \theta_2}{\partial \alpha_1} - \frac{\theta_1}{A_1 A_2}\frac{\partial A_1}{\partial \alpha_2}, \qquad \kappa_4 = \frac{1}{A_2}\frac{\partial \theta_1}{\partial \alpha_2} - \frac{\theta_2}{A_1 A_2}\frac{\partial A_2}{\partial \alpha_1}.$$

2.3. Constitutive Relations

It is assumed that the material is elastic. The constitutive relations for a unidirectional lamina with respect to material axes $(\overline{\alpha}_1, \overline{\alpha}_2)$ can be written as:

$$\{\overline{\sigma}\} = [\overline{Q}]\{\overline{\varepsilon}\}. \tag{5}$$

Equation (5) can be written in expanded form as:

$$\begin{Bmatrix} \overline{\sigma}_{11} \\ \overline{\sigma}_{22} \\ \overline{\tau}_{12} \\ \overline{\tau}_{13} \\ \overline{\tau}_{23} \end{Bmatrix}_k = \begin{bmatrix} \overline{Q}_{11} & \overline{Q}_{12} & 0 & 0 & 0 \\ \overline{Q}_{21} & \overline{Q}_{22} & 0 & 0 & 0 \\ 0 & 0 & \overline{Q}_{66} & 0 & 0 \\ 0 & 0 & 0 & k_s\overline{Q}_{44} & 0 \\ 0 & 0 & 0 & 0 & k_s\overline{Q}_{55} \end{bmatrix}_k \left(\begin{Bmatrix} \overline{\varepsilon}_{11} \\ \overline{\varepsilon}_{22} \\ \overline{\gamma}_{12} \\ \overline{\gamma}_{13} \\ \overline{\gamma}_{23} \end{Bmatrix}_k \right). \tag{6}$$

The shear correction factor (k_s) is assumed to be 5/6. The off-axis constitutive relations for kth lamina is:

$$\begin{Bmatrix} \sigma_{11} \\ \sigma_{11} \\ \tau_{12} \\ \tau_{23} \\ \tau_{23} \end{Bmatrix}_k = \begin{bmatrix} Q_{11} & Q_{12} & Q_{16} & 0 & 0 \\ Q_{21} & Q_{22} & Q_{26} & 0 & 0 \\ Q_{16} & Q_{26} & Q_{66} & 0 & 0 \\ 0 & 0 & 0 & k_s Q_{44} & k_s Q_{45} \\ 0 & 0 & 0 & k_s Q_{45} & k_s Q_{55} \end{bmatrix}_k \left(\begin{Bmatrix} \varepsilon_{11} \\ \varepsilon_{22} \\ \gamma_{12} \\ \gamma_{13} \\ \gamma_{23} \end{Bmatrix}_k \right), \tag{7}$$

where Q_{ij} are the transformed coefficients [15]. The force and moment resultants are obtained by integrating the stresses and their moments through the laminate thickness as given by

$$\begin{Bmatrix} N_{11}, & M_{11} \\ N_{22}, & M_{22} \\ N_{12}, & M_{12} \end{Bmatrix} = \int_{-h/2}^{+h/2} \begin{Bmatrix} \sigma_{11} \\ \sigma_{22} \\ \tau_{12} \end{Bmatrix} (1, \zeta)\, \mathrm{d}\zeta = \sum_{k=1}^{N} \int_{\zeta_{k-1}}^{\zeta_k} \begin{Bmatrix} \sigma_{11} \\ \sigma_{22} \\ \tau_{12} \end{Bmatrix} (1, \zeta)\, \mathrm{d}\zeta,$$
$$\begin{Bmatrix} Q_{13} \\ Q_{23} \end{Bmatrix} = \int_{-h/2}^{+h/2} \begin{Bmatrix} \tau_{13} \\ \tau_{23} \end{Bmatrix} \mathrm{d}\zeta = \sum_{k=1}^{N} \int_{\zeta_{k-1}}^{\zeta_k} \begin{Bmatrix} \tau_{13} \\ \tau_{23} \end{Bmatrix} \mathrm{d}\zeta, \tag{8}$$

where N_{11}, N_{22} and N_{12} are the in-plane force resultants; M_{11}, M_{22} and M_{12} are the moment resultants; Q_{13} and Q_{23} are the transverse shear resultants. In compact form, force and moment resultants can be written as

$$\{F\} = [D]\{\varepsilon\}, \tag{9}$$

where $[D]$ is the elasticity matrix (see Appendix A) and

$$\{F\} = \{\, N_{11} \quad N_{22} \quad N_{12} \quad M_{11} \quad M_{22} \quad M_{12} \quad Q_{13} \quad Q_{23} \,\}^{\mathrm{T}},$$
$$\{\varepsilon\} = \{\, \varepsilon^0_{11} \quad \varepsilon^0_{22} \quad \gamma^0_{12} \quad \kappa_{11} \quad \kappa_{22} \quad \kappa_{12} \quad \gamma^0_{13} \quad \gamma^0_{23} \,\}^{\mathrm{T}}. \tag{10}$$

The isoparametric formulation [16] has been used to implement the nine-noded shell element, where each node has five degrees of freedom, $u_1^0, u_2^0, w^0, \theta_1$ and θ_2. The displacement components at any point on the mid-surface are assumed as:

$$\begin{aligned} u_1^0 &= \sum_{i=1}^{9} N_i u_{1i}^0, \qquad u_2^0 = \sum_{i=1}^{9} N_i u_{2i}^0, \qquad w^0 = \sum_{i=1}^{9} N_i w_i^0, \\ \theta_1 &= \sum_{i=1}^{9} N_i \theta_{1i} \quad \text{and} \quad \theta_2 = \sum_{i=1}^{9} N_i \theta_{2i}. \end{aligned} \tag{11}$$

The above can be expressed in a matrix form given by

$$\{u\} = [N]\{\delta\}, \tag{12}$$

where

$$\{u\} = \{\, u_1^0 \quad u_2^0 \quad w^0 \quad \theta_1 \quad \theta_2 \,\}^{\mathrm{T}}, \qquad \{\delta\} = \{\, u_{1i}^0 \quad u_{1i}^0 \quad w_i^0 \quad \theta_{1i} \quad \theta_{2i} \,\}^{\mathrm{T}} \tag{13}$$

and

$$[N] = \begin{bmatrix} N_i & 0 & 0 & 0 & 0 \\ 0 & N_i & 0 & 0 & 0 \\ 0 & 0 & N_i & 0 & 0 \\ 0 & 0 & 0 & N_i & 0 \\ 0 & 0 & 0 & 0 & N_i \end{bmatrix}_{i=1,2,\ldots,9}, \tag{14}$$

N_i represents the shape function of ith node of an element.

2.4. Principle of Virtual Work

The equations of motion are derived using the principle of virtual work:

$$dW = dW_{\mathrm{int}} - dW_{\mathrm{ext}} = 0, \tag{15}$$

where

$$\begin{aligned} dW_{\mathrm{int}} &= \int_V \{d\varepsilon\}^{\mathrm{T}}\{\sigma\}\,\mathrm{d}V \\ &= \int_V \left(\{d\varepsilon_l^0\}^{\mathrm{T}}\{N\} + \{d\varepsilon_{nl}^0\}^{\mathrm{T}}\{N\} + \{d\kappa\}^{\mathrm{T}}\{M\} + \{d\gamma^0\}\{Q\}\right)\mathrm{d}A \\ &= \{d\delta\}^{\mathrm{T}}\left([K_l] + \frac{1}{2}[N_1] + \frac{1}{3}[N_2]\right)\{\delta\} - \{d\delta\}^{\mathrm{T}}\{R\}, \end{aligned} \tag{16}$$

$$\begin{aligned} dW_{\mathrm{ext}} &= \int_A \big[-I_1\big(\{\ddot{u}_1^0\}\{du_1^0\} + \{\ddot{u}_1^0\}\{du_2^0\} + \{\ddot{w}\}\{dw\}\big) \\ &\qquad - I_2\big(\{\ddot{\theta}_1\}\{d\ddot{\theta}_1\} - I_3\{\ddot{\theta}_2\}\{d\ddot{\theta}_2\}\big) + p\,d\delta\big]\,\mathrm{d}A \\ &= -\{d\delta\}^{\mathrm{T}}[M]\{\ddot{\delta}\} + \{d\delta\}^{\mathrm{T}}\{R\}, \end{aligned} \tag{17}$$

where d is the variation operator, $\{\delta\}$ is the displacement vector, $[K_1]$ is the linear stiffness matrix, $[N_1]$ and $[N_2]$ are the first and second-order non-linear stiffness matrices due to large deformation; $\{R\}$ is the external force vectors:

$$\begin{aligned}
[K_l] &= \int_A \left([B_l]^{\mathrm{T}}[D][B_l]\right) \mathrm{d}A, \\
[N_1] &= \int_A \left([B_l]^{\mathrm{T}}[D][B_{nl}] + [B_{nl}]^{\mathrm{T}}[D][B_l] + [G]^{\mathrm{T}}[S_l][G]\right) \mathrm{d}A, \\
[N_2] &= \int_A \left([B_{nl}]^{\mathrm{T}}[D][B_{nl}] + [G]^{\mathrm{T}}[S_{nl}][G]\right) \mathrm{d}A, \\
[M] &= \int_A [N]^{\mathrm{T}}\hat{\rho}[N] \, \mathrm{d}A,
\end{aligned} \tag{18}$$

and $[M]$, $[G]$ and $[S]$ matrices are expressed in Appendix A.

Substituting the equations (17) and (18) into equation (16), the governing equilibrium is as follows:

$$[M]\{\ddot{\delta}\} + \left([K] + \frac{1}{2}[N_1] + \frac{1}{3}[N_2]\right)\{\delta\} = \{R\}. \tag{19}$$

For the analysis of free vibration of buckled laminated shells, the displacement vector is assumed to be the sum of time-dependent $\{\delta_{\mathrm{t}}\}$ and time-independent $\{\delta_{\mathrm{s}}\}$ displacement components. The magnitude of time-dependent solution $\{\delta_{\mathrm{t}}\}$ is small and the magnitude of the time-independent solution $\{\delta_{\mathrm{s}}\}$ is large. However, $\{\delta_{\mathrm{s}}\}$ is the post-bucking large deflection and the non-linear stiffness matrices are functions of the time-independent displacement $\{\delta_{\mathrm{s}}\}$. The static and dynamic coupled equations are:

$$\{\psi\} = \left(K_l + \frac{1}{2}N_1(\delta_{\mathrm{s}}) + \frac{1}{3}N_2(\delta_{\mathrm{s}})\right)\delta_{\mathrm{s}} - \lambda R = 0, \tag{20}$$

$$M\{\ddot{\delta}_{\mathrm{t}}\} + \left(K_l + N_1(\delta_{\mathrm{s}}) + N_2(\delta_{\mathrm{s}})\right)\delta_{\mathrm{t}} = 0. \tag{21}$$

The arc-length method [12] is used to solve non-linear problems, and the incremental iterative form of equation (21) can be expressed as:

$$\left(K_l + N_1(\delta_{\mathrm{s}}) + N_2(\delta_{\mathrm{s}})\right)\{d\delta_{\mathrm{s}}\}^{i+1} = \lambda\{R\}^i - \{F\}^i, \tag{22}$$

where $\{F\}$ is the force vector due to internal stresses due to loading. After solving equation (23), the updated displacements vector is determined as follows:

$$\{\delta_{\mathrm{s}}\}_{n+1}^{(i+1)} = \{\delta_{\mathrm{s}}\}_{n+1}^{(i)} + \{d\delta\}_n^{(i)}. \tag{23}$$

After obtaining the converged post-buckling deflection, the vibration analysis is carried out by solving a generalized eigenvalue problem as,

$$\left[\left(K_l + N_1(\delta_{\mathrm{s}}) + N_2(\delta_{\mathrm{s}})\right)\delta_{\mathrm{t}} - \omega^2 M\right]\{\delta_{\mathrm{t}}\} = 0. \tag{24}$$

Typical cylindrical and spherical shell panels are shown in Figs 4 and 5, respectively. The shell panel dimensions of a and b are along the α_1 and α_2 directions,

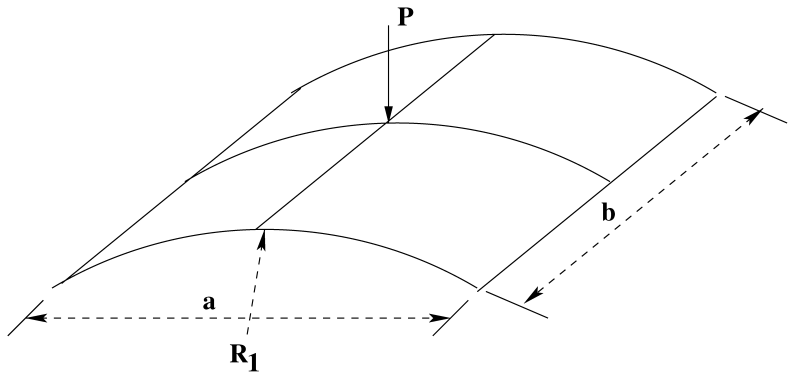

Figure 4. A typical cylindrical panel.

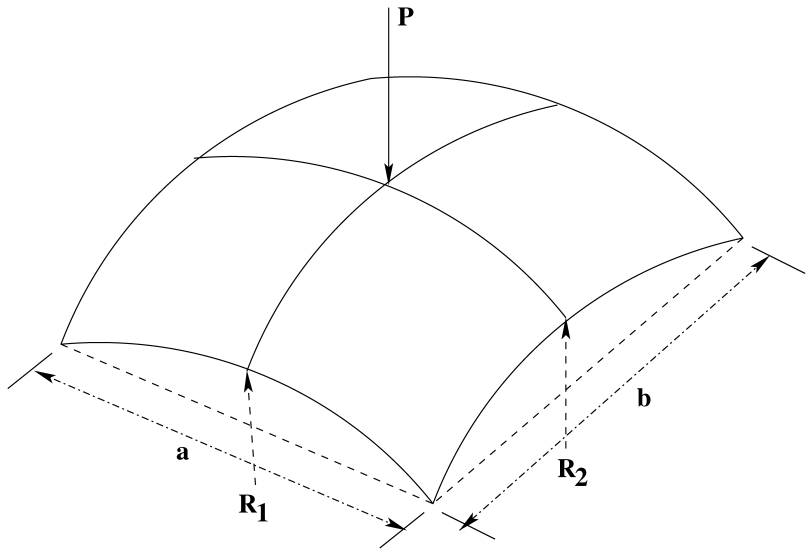

Figure 5. A typical spherical panel.

respectively. The boundary conditions used for all simply supported are as follows:

$$\begin{aligned} u_2^0 = w = \theta_2 = 0, \quad & \text{for } \alpha_1 = 0, a, \\ u_1^0 = w = \theta_1 = 0, \quad & \text{for } \alpha_2 = 0, b. \end{aligned} \tag{25}$$

The non-dimensional frequency is defined as:

$$\Omega = \omega \frac{a^2}{h} \sqrt{\frac{\rho}{E_{22}}}, \tag{26}$$

where ω is the fundamental frequency, ρ is the mass density of the laminate, E_{22} is the Young's modulus. The vibration analysis on the region with non-positive stiffness matrix is skipped. A finite element code in C++ language is written to im-

plement the above finite element formulation. The code is first validated and then employed to generate numerical results.

3. Results and Discussion

3.1. Comparison of Results

To evaluate the efficiency and validity of the present formulation, a variety of snapping and free vibration problems are considered.

3.1.1. Isotropic Cylindrical Panel

The post-buckling behavior of a hinged isotropic cylindrical panel under action of a concentrated point load is considered. The geometric and material properties of the shell are $a = b = 508$ mm, $R = 2540$ mm, $h = 6.35$ mm, $E = 3103$ N/mm^2 and $\nu = 0.3$. Due to the symmetric nature of the problem, only one-quarter of the panel is considered for the finite element discretization. The present non-linear central load–deflection curves are compared with those obtained by Sabir and Djoudi [17] and Crisfield [12] and are presented in Fig. 6. The present results compare well with the published results.

3.1.2. Laminated Cylindrical Panel

Next, snap-through behavior of cross-ply laminated cylindrical shell panels subjected to a central point load is analyzed. The following two different laminates are considered: [90/0/90] and [0/90/0]. The geometric and material data and also the boundary conditions of the cylindrical panel are the same as in the previously

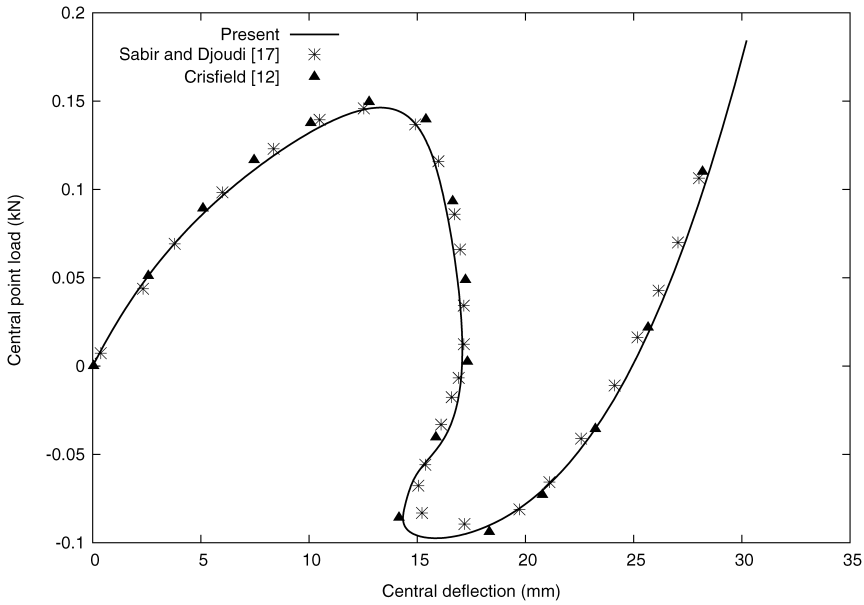

Figure 6. Snap-through response of isotropic cylindrical panel.

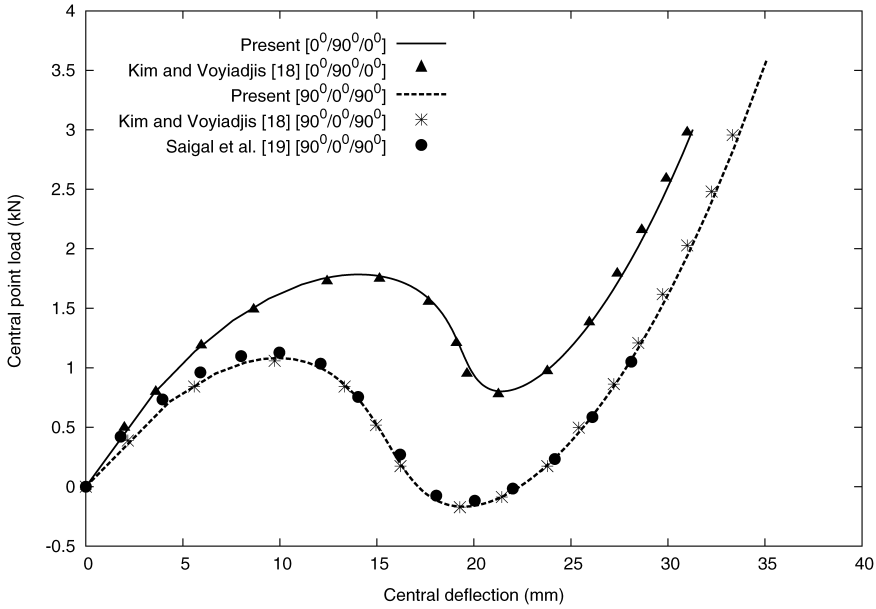

Figure 7. Snap-through response of laminated cylindrical panels.

discussed problem. The present results are compared with the results obtained by Kim and Voyiadjis [18] for the [0/90/0] laminate. The finite element used by Kim and Voyiadjis [18] is an eight-noded shell element with six degrees of freedom per node. For the [90/0/90] laminate, the present results are compared with the results obtained by Kim and Voyiadjis [18] and Saigal *et al.* [19]. All the pre/post-buckling load–deflection curves are shown in Fig. 7. The results given by Saigal *et al.* [19] are based on a four-nodded non-linear shell element with twelve degrees of freedom. The present results and the published results are in very good agreement.

3.1.3. Free Vibration Analysis

A simply supported square plate is considered. The results are predicted by the present formulation for different modulus ratios are compared with the 3D solution of Noor [20], Chandrashekhara [21] and classical plate theory results are shown in Table 1. Table 2 shows the fundamental frequencies of clamped [0/90] laminated spherical shell panel ($a = b = 10.0$ in, $h = 0.1$ in). The material properties used in this example are as follows:

$$E_{11} = 21 \times 10^6 \text{ psi}, \qquad E_{22} = 1.4 \times 10^6 \text{ psi}, \qquad G_{12} = G_{13} = 0.6 \times 10^6 \text{ psi},$$
$$G_{23} = 0.5 \times 10^6 \text{ psi}, \qquad \nu_{12} = 0.3, \qquad \rho = 0.0001475 \text{ lb/in}^3.$$

The present results are in good agreement with the published results as shown in Tables 1 and 2.

3.2. Snapping and Vibration Characteristics of Cylindrical Shell Panel

In order to perform the convergence study, a simply supported symmetric [0/90/

Table 1.
Effect of degree of orthotropy on the non-dimensional fundamental frequencies $\overline{\omega} = \omega(\rho h^2/E_{22})^{1/2}$ of [0/90/0/90] simply supported square plate

E_{11}/E_{22}	Classical plate theory [21]	Noor [20]	Chandashekhara [21]	Present
3	0.28676	0.26182	0.26348	0.25787
10	0.38877	0.32578	0.34026	0.32434
20	0.49907	0.37622	0.40198	0.37992
30	0.58900	0.40660	0.43954	0.41476

Table 2.
Fundamental frequencies (Hz) of clamped [0/90] spherical shell panel

R/a	Chandashekhara [21]	Present
10	590.59	590.29
20	380.27	380.29
30	325.46	325.56
40	303.84	303.99

90/0] laminated cylindrical panel is subjected to a point load at the center of the panel. The geometric properties are as follows:

$$a = b = 100 \text{ mm}, \qquad a/h = 150, \qquad R/a = 5.$$

The material properties are considered as:

$$E_{11} = 181 \text{ GPa}, \qquad E_{22} = 10.3 \text{ GPa}, \qquad G_{12} = G_{13} = 7.17 \text{ GPa},$$
$$G_{23} = 3.58 \text{ GPa}, \qquad \nu_{12} = 0.28, \qquad \rho = 1600 \text{ kg/m}^3.$$

The cylindrical panel is discretized into different mesh sizes ($2 \times 2, 4 \times 4, 8 \times 8, 10 \times 10$ and 12×12). The vibration characteristics of pre/post-buckled panels are shown in Fig. 8. It is observed that the vibration characteristics of post-buckled shell panels having mesh size ($8 \times 8, 10 \times 10$ and 12×12) have nearly the same results. The present numerical analysis is carried out for full composite shell panel having mesh size (8×8).

The effects of thickness on post-buckling behavior of a simply supported cylindrical panel ($a = b = 100$ mm and $R/a = 5$) are considered for different values of a/h, such as 100, 125, 150, 175 and 200. The lamination scheme is anti-symmetric cross-ply $[0/90]_2$ with four layers. The non-linear load–deflection curves are shown in Fig. 9. It is observed that as the thickness of the shell panel decreases the limit point load for buckling decreases. A thicker shell undergoes post-buckling at a higher limit point load compare to the thinner shell, and the thinner shell exhibits snap-through and snap-back phenomena. At the limit point, the determinate of the

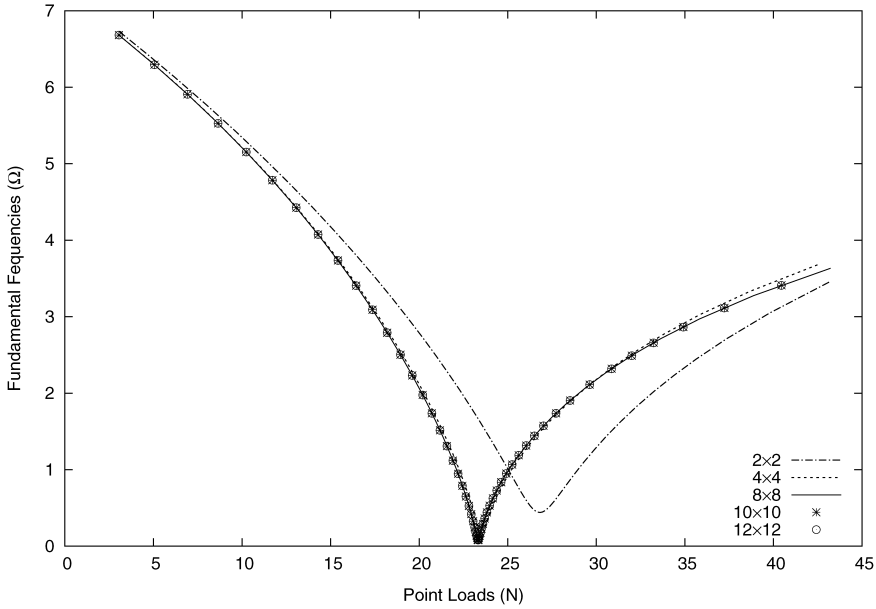

Figure 8. Convergence study of [0/90/90/0] laminated cylindrical panel.

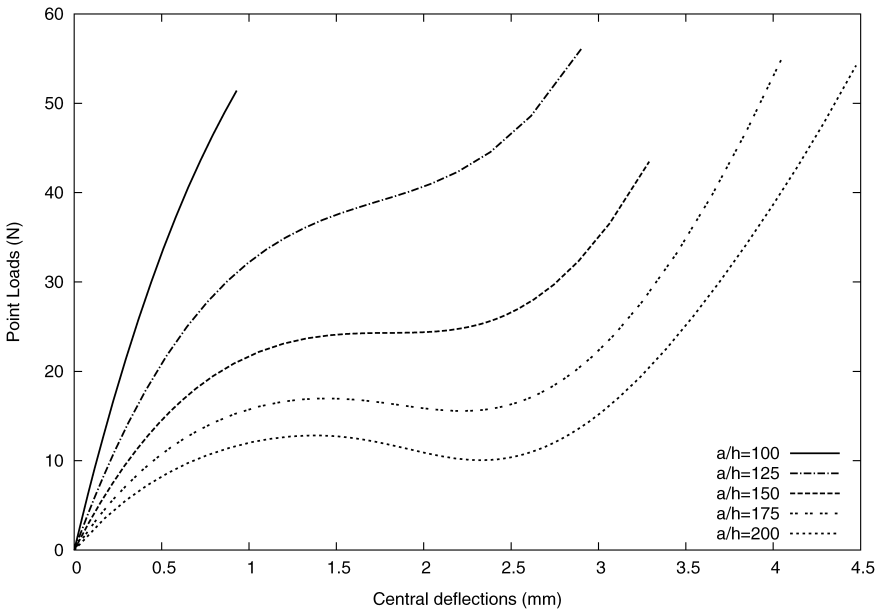

Figure 9. Effect of thickness ratio on snapping behavior of $[0/90]_2$ laminated cylindrical panel.

stiffness matrix is zero. After snap-through, the load carrying capacity increases due to the post-buckling strength of the shell. The snapping behavior is observed due to the sudden transfer of energy from membrane to bending component. This

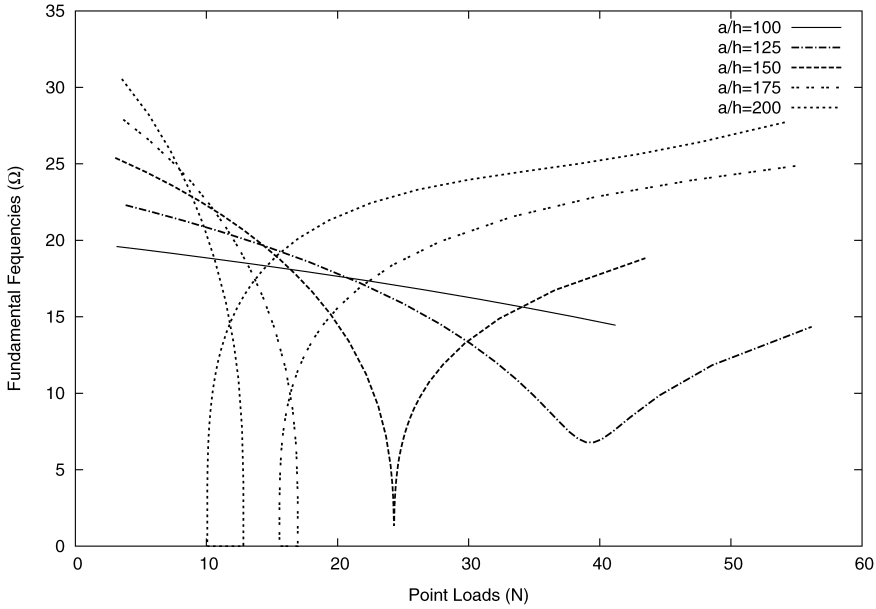

Figure 10. Effect of thickness ratio on vibration characteristics of $[0/90]_2$ laminated cylindrical panel.

phenomenon is dynamic in nature. The vibration characteristics of a cylindrical panel for different a/h values are shown in Fig. 10. The fundamental frequency response can be separated into pre-buckling and post-buckling regions and the vibration analysis on the region with non-positive stiffness is skipped. It is observed that the frequencies in the pre-snapping region decrease with the increase in load. But after snap-through, the frequencies increase as the load increases, due to the geometric non-linearity. The rate of change in fundamental frequency depends on the thickness of the shell. The snapping phenomena affect the vibration characteristics as well as static deformation.

The effects of radius of curvature of an anti-symmetric $[0/90]_2$ laminated cylindrical panel ($a = b = 100$ mm and $a/h = 150$) on snapping behavior are shown in Fig. 11. Various R/a values are considered, such as 5, 6, 7, 8, 9 and 10. It is observed that, as the radius of curvature increases, the limit point load decreases. In the case of a curved panel, both bending and membrane stiffness are responsible to carry loads and membrane stiffness dominant bending stiffness before snap-through occurs. With the increase in shallowness, the snapping phenomena appear and the membrane stiffness dominant bending stiffness due to decrease in curvature. For $R/a = 5$, the snapping phenomenon is more significant compared with higher values of R/a (6, 7, 8, 9 and 10). Figure 12 shows the variation of fundamental frequencies with respect to the applied loads. The fundamental frequencies decrease in the pre-buckling region and increase in post-buckling region. The rate of change of fundamental frequency depends on the radius of curvature of the shell panel. For

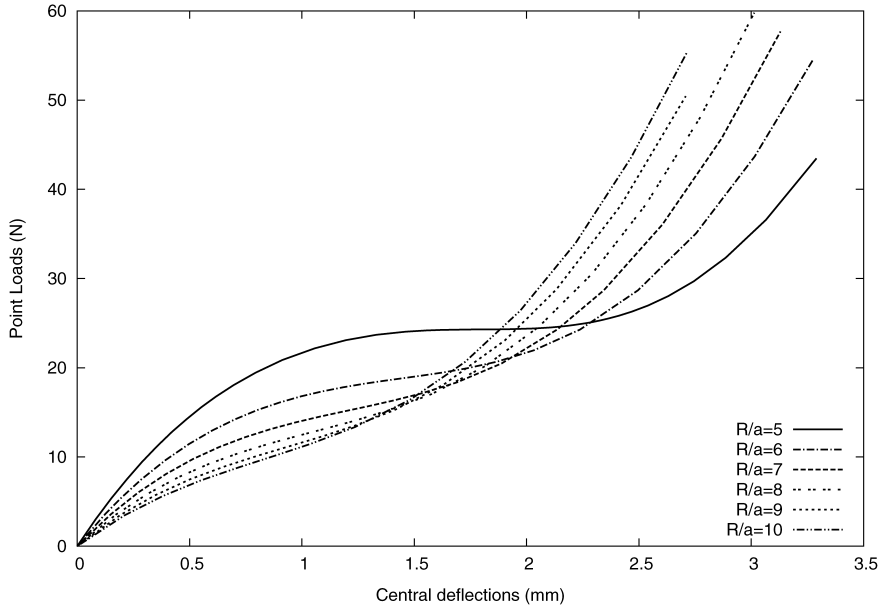

Figure 11. Effect of shallowness on snapping behavior of $[0/90]_2$ laminated cylindrical panel.

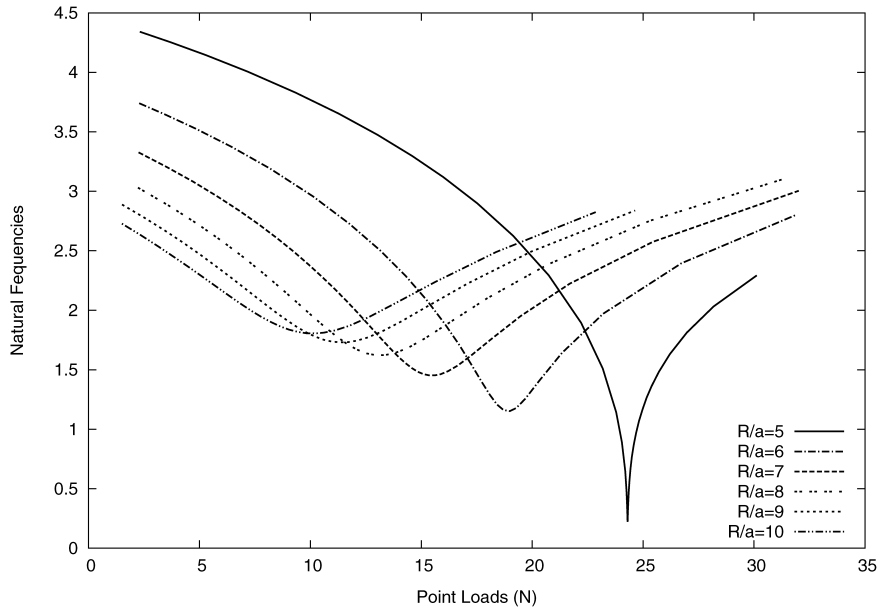

Figure 12. Effect of shallowness on vibration characteristics of $[0/90]_2$ laminated cylindrical panel.

$R/a = 5$ there is a sudden increase in frequency due to the snapping behavior of the panel. For higher value of R/a, the fundamental frequency curve has a dip.

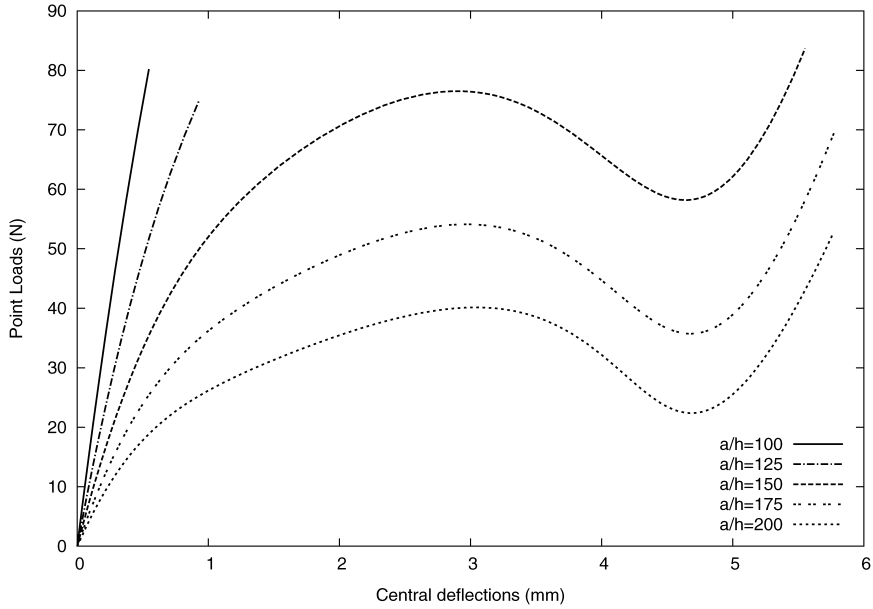

Figure 13. Effect of thickness ratio on snapping behavior of $[0/90]_2$ laminated spherical panel.

3.3. Snapping and Vibration Characteristics of Spherical Shell Panel

A simply supported spherical panel subjected to a point load at the center is analyzed for the post-buckling and vibration analysis. The material properties are same as the cylindrical shell discussed in the earlier section. The following material properties are used:

$$a = b = 100.0 \text{ mm}, \qquad R_1 = R_2 = 500 \text{ mm}.$$

To investigate the effect of thickness ratio (a/h), different thickness ratios such as $a/h = 100, 125, 150, 175$ and 200 are considered. The lamination scheme is anti-symmetric cross-ply $[0/90]_2$ with four layers. The thickness effects on post-buckling behaviour of spherical panel are shown in Fig. 13. It is observed that as the thickness of the panel decreases the limit point load for buckling decreases. Figure 14 shows the vibration characteristics of cylindrical panels of different a/h values. Snap-through phenomena were observed at different point loads for different a/h values. A spherical shell shows a higher limit point load compared to the cylindrical panel due to the curvatures on both sides of the spherical panel.

The effects of shallowness of a doubly curved shell panel ($a = b = 100$ mm, $a/h = 150$) are considered next. Various R/a value are considered, such as 5, 6, 7, 8, 9, 10, 15 and 20. The load–deflection curves are shown in Fig. 15. It is observed that, as the radius of curvature increases, the limit point load decreases. For $R/a = 5$, the snapping phenomenon is more significant compared with higher values of R/a (6, 7, 8, 9, 10, 15 and 20). Figure 16 shows the variation of fundamental

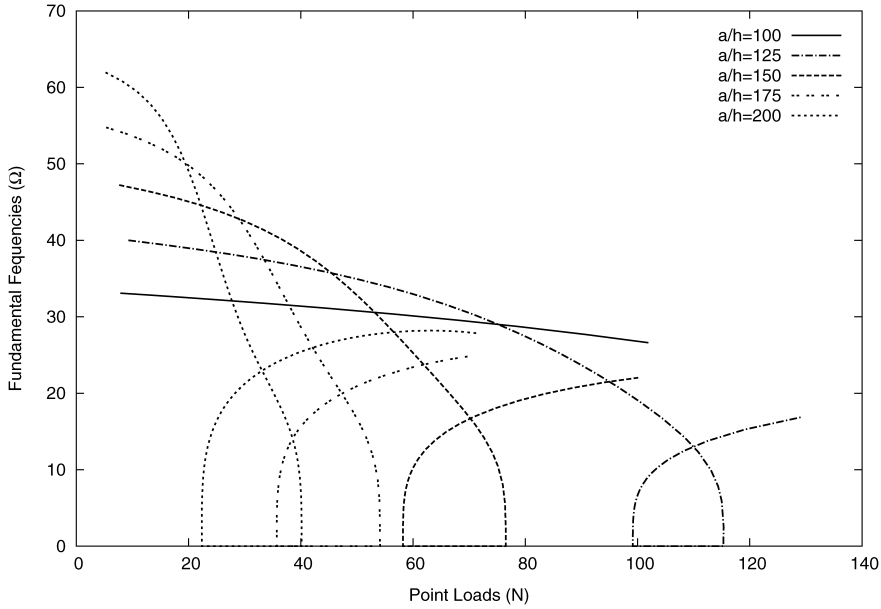

Figure 14. Effect of thickness ratio on vibration characteristics of $[0/90]_2$ laminated spherical panel.

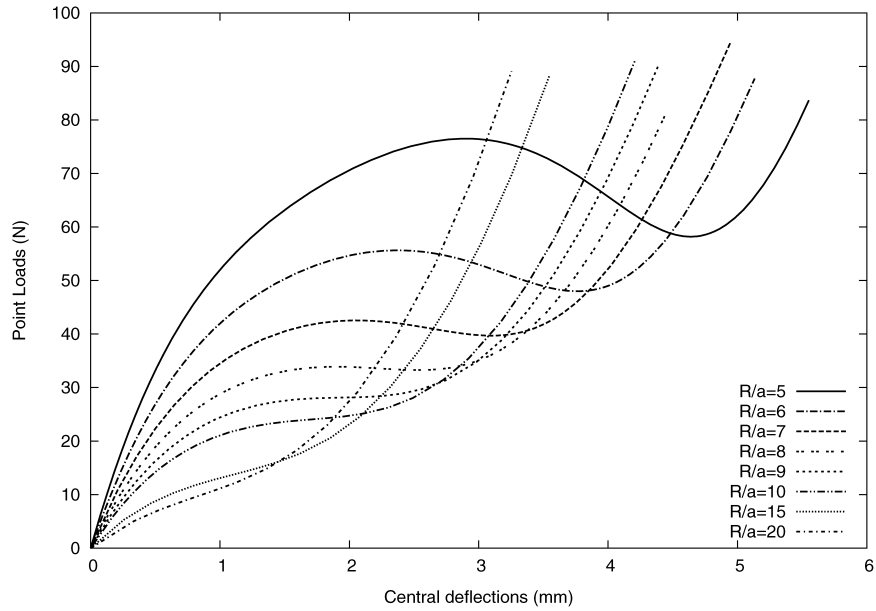

Figure 15. Effect of shallowness on snapping behavior of $[0/90]_2$ laminated spherical panel.

frequencies with respect to the applied loads. The fundamental frequencies decrease in the pre-buckling region and increase in the post-buckling region.

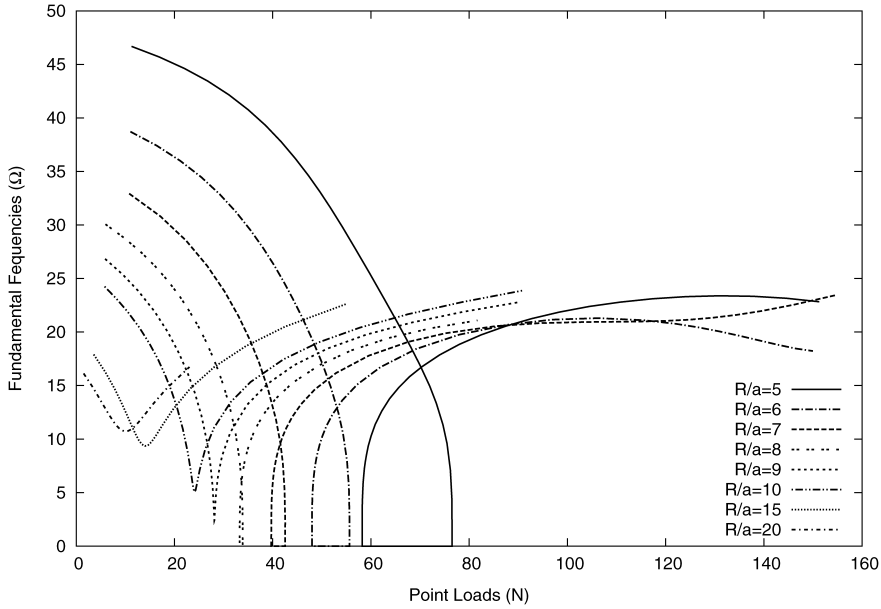

Figure 16. Effect of shallowness on vibration characteristics of $[0/90]_2$ laminated spherical panel.

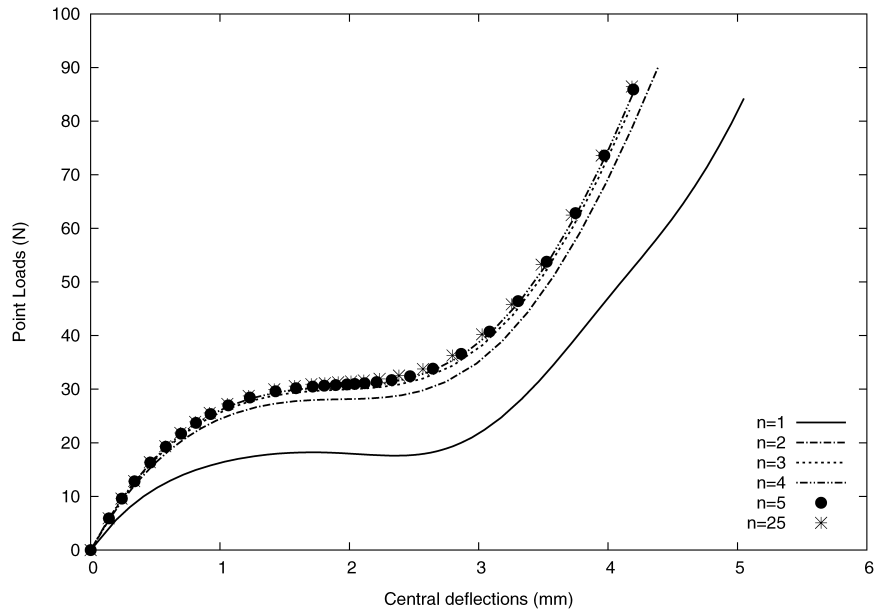

Figure 17. Effect of number of layers on snapping behavior of $[0/90]_n$ laminated spherical panel.

A simply supported $[0/90]_n$ laminated spherical panel is considered for $n = 1, 2, 3, 4, 5$ and 25. The load–deflection curves are shown in Fig. 17 and the frequency responses with respect to the applied loads are shown in Fig. 18. The limit

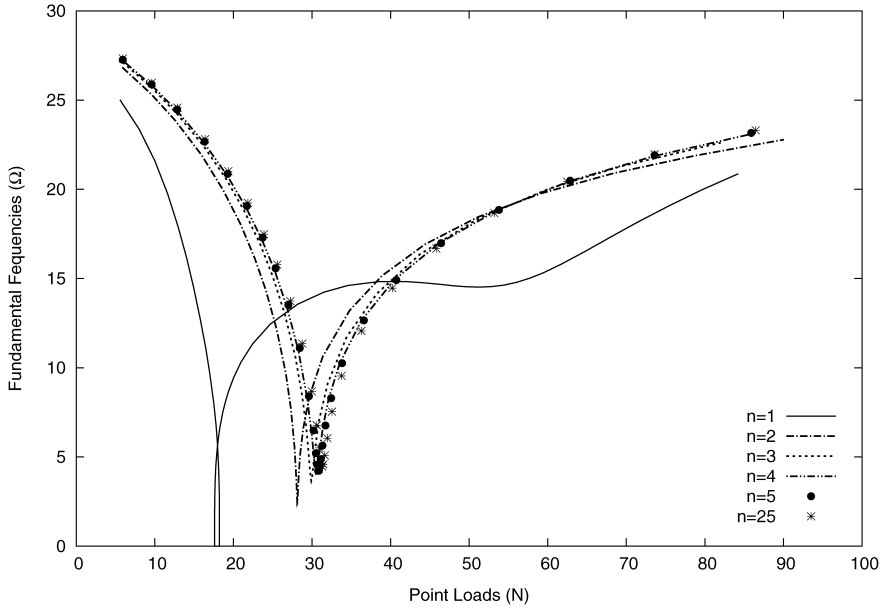

Figure 18. Effect of number of layer on vibration characteristics of $[0/90]_n$ laminated spherical panel.

point load for $n = 1$ is found to be lower compared to the higher values of n. As the number of layers (n) increases, the limit point load increases due to the higher coupling effects between bending and extension. However, it is observed that there are very small differences in limit point loads and fundamental frequencies for $n = 3, 4, 5$ and 25. When the value of n is increased beyond 4, the coupling stiffness between bending and extension converge.

4. Conclusion

The non-linear finite element method has been employed to examine the vibration characteristics of pre- and post-buckled laminated composite doubly curved shells:

1. The strain–displacement relations used are of the general form. If the linear in-plane membrane strains are much smaller then out-of-plane rotation about the normal to the reference surface, then the present strain–displacement relations can be reduced to Sanders and Donnell non-linear strains.

2. Both deep and shallow shell surfaces can be modeled using nine-noded doubly curved shell element and the non-linear finite element formulation is presented in a curvilinear coordinates system. Different types of shells, such as spherical, cylindrical, conical, hyperbolic, parabolic and other types of shells can be analyzed.

3. Arc-length method is implemented to capture the snapping phenomenon accurately. The vibration characteristics of post-buckled shell are performed using

tangent stiffness obtained from the converged deflection. Good agreement is observed between the present and published results.

4. The fundamental frequency response is separated into pre-buckling and post-buckling regions. It is observed that the frequency in the pre-snapping region decreases with increase in load. But after snap-through, the frequency increases with increase in load, due to the geometric non-linearity.

5. The coupling between bending and extension in anti-symmetric laminated shells play an important role in the study of the snapping and vibration characteristics. Therefore, the present results represent valuable information for the understanding of the dynamics of complex thin-walled structures, which exhibit post-buckling behavior.

Acknowledgement

This work was supported by Defense Acquisition Program Administration and Agency for the Defense Development under the contract UD060009AD. The first author thanks the support of the second stage of the Brain Korea 21 project in 2007.

References

1. R. D. Wood and O. C. Zienkiewicz, Geometrically nonlinear finite element analysis of beams, frames, arches and axisymmetric shells, *Computers and Structures* **7**, 725–735 (1977).
2. K. J. Bathe, E. Ramm and E. L. Wilson, Finite element formulations for large deformation dynamic analysis, *Intl. J. Numer. Methods Engng* **9**, 353–386 (1975).
3. S. Ilanko and S. M. Dickinson, The vibration and post-buckling of geometrically imperfect, simply supported, rectangular plates under uni-axial loading, Part I: Theoretical approach, *J. Sound Vibr.* **118**, 313–336 (1987).
4. A. N. Palazotto and P. E. Linnemann, Vibration and buckling characteristics of composite cylindrical panels incorporating the effects of a higher order shear theory, *Intl. J. Solids Struct.* **28**, 341–361 (1991).
5. M. A. Souza, Vibration of thin-walled structures with asymmetric post-buckling characteristics, *Thin-Walled Structures* **14**, 45–57 (1992).
6. D. Lee and I. Lee, Vibration behaviors of thermally post-buckled anisotropic plates using first-order shear deformable plate theory, *Compos. Struct.* **63**, 371–378 (1997).
7. I. K. Oh, J. H. Han and I. Lee, Post-buckling and vibration characteristics of piezolaminated composite plate subject to thermopiezoelectric loads, *J. Sound Vibr.* **233**, 19–40 (2000).
8. H. Chen and W. Yu, Post-buckling and mode jumping analysis of composite laminates using an asymptotically correct, geometrically non-linear theory, *Intl. J. Non-Linear Mech.* **41**, 1143–1160 (2006).
9. J. G. Teng and T. Hong, Nonlinear thin shell theories for numerical buckling predictions, *Thin-Walled Structures* **31**, 89–115 (1998).
10. C. K. Kundu and P. K. Sinha, Post-buckling analysis of laminated composite shells, *Compos. Struct.* **78**, 316–324 (2007).
11. A. K. Jha and D. J. Inman, Importance of geometric nonlinearity and follower pressure load in the dynamic analysis of a gossamer structure, *J. Sound Vibr.* **278**, 207–231 (2004).

12. M. A. Crisfield, A fast incremental iterative solution procedure that handles snap through, *Computers and Structures* **13**, 55–62 (1981).
13. H. Kraus, *Thin Elastic Shells*. John Wiley and Sons, New York, USA (1967).
14. A. S. Saada, *Elasticity: Theory and Applications*. Pergamon Press, New York, USA (1974).
15. R. Jones, *Mechanics of Composite Materials*. Taylor and Francis, Philadelphia, USA (1999).
16. O. C. Zienkiewicz and R. L. Taylor, *The Finite Element Method*, Vol. 1. McGraw Hill International Edition, Singapore (1989).
17. A. B. Sabir and M. S. Djoudi, Shallow shell finite element for the large deformation geometrically nonlinear analysis of shells and plates, *Thin-Walled Structures* **21**, 253–267 (1995).
18. K. Kim and G. Z. Voyiadjis, Nonlinear finite element analysis of composite panels, *Composites: Part B* **30**, 365–381 (1999).
19. S. Saigal, R. K. Kapania and T. Y. Yang, Geometrically nonlinear finite element analysis of imperfect laminated shells, *J. Compos. Mater.* **20**, 197–214 (1986).
20. A. K. Noor, Free vibrations of multilayered composite plates, *AIAA Journal* **7**, 1038–1039 (1973).
21. K. Chandrashekhara, Free vibration of anisotropic laminated doubly curved shells, *Computers and Structures* **33**, 435–440 (1989).

Appendix

The elasticity matrix is as follows:

$$[D] = \begin{bmatrix} A_{11} & & & & & & & \\ A_{12} & A_{22} & & & & \text{Sym} & & \\ A_{16} & A_{26} & A_{66} & & & & & \\ B_{11} & B_{12} & B_{16} & D_{11} & & & & \\ B_{12} & B_{22} & B_{26} & D_{12} & D_{22} & & & \\ B_{16} & B_{26} & B_{66} & D_{16} & D_{26} & D_{66} & & \\ 0 & 0 & 0 & 0 & 0 & 0 & A_{44} & \\ 0 & 0 & 0 & 0 & 0 & 0 & A_{45} & A_{55} \end{bmatrix}, \tag{A.1}$$

where A_{ij}, B_{ij} and D_{ij} are the extension, bending-stretching coupling, bending terms, respectively and are as expressed as follows:

$$\begin{aligned} A_{ij} &= \sum_{k=1}^{N} [Q_{ij}]_k (\zeta_k - \zeta_{k-1}), \quad i, j = 1, 2, 6, \\ B_{ij} &= \frac{1}{2} \sum_{k=1}^{N} [Q_{ij}]_k (\zeta_k^2 - \zeta_{k-1}^2), \quad i, j = 1, 2, 6, \\ D_{ij} &= \frac{1}{3} \sum_{k=1}^{N} [Q_{ij}]_k (\zeta_k^3 - \zeta_{k-1}^3), \quad i, j = 1, 2, 6, \\ A_{ij} &= \sum_{k=1}^{N} [Q_{ij}]_k (\zeta_k - \zeta_{k-1}), \quad i, j = 4, 5. \end{aligned} \tag{A.2}$$

The detailed component matrices of stiffness matrices are presented as follows:

The mass stiffness matrix is as follows:

$$[M] = \int_A [N]^{\mathrm{T}} \hat{\rho} [N] \, \mathrm{d}A, \tag{A.3}$$

where $[N]$ is expressed in equation (14).

$$[\hat{\rho}] = \begin{bmatrix} I_1 & 0 & 0 & I_2 & 0 \\ 0 & I_1 & 0 & 0 & I_2 \\ 0 & 0 & I_1 & 0 & 0 \\ I_2 & 0 & 0 & I_3 & 0 \\ 0 & I_2 & 0 & 0 & I_3 \end{bmatrix}, \tag{A.4}$$

where $(I_1, I_2, I_3) = \int_{-h/2}^{h/2} \rho(1, \zeta, \zeta^2) \, \mathrm{d}\zeta$.

$$[G] = \begin{bmatrix} \dfrac{1}{A_1}\dfrac{\partial N_i}{\partial \alpha_1} & \dfrac{N_i}{A_1 A_2}\dfrac{\partial A_1}{\partial \alpha_2} & \dfrac{N_i}{R_1} & 0 & 0 \\ \dfrac{1}{A_2}\dfrac{\partial N_i}{\partial \alpha_2} & -\dfrac{N_i}{A_1 A_2}\dfrac{\partial A_2}{\partial \alpha_1} & 0 & 0 & 0 \\ -\dfrac{N_i}{A_1 A_2}\dfrac{\partial A_1}{\partial \alpha_2} & \dfrac{1}{A_1}\dfrac{\partial N_i}{\partial \alpha_1} & 0 & 0 & 0 \\ \dfrac{N_i}{A_1 A_2}\dfrac{\partial A_2}{\partial \alpha_1} & \dfrac{1}{A_2}\dfrac{\partial N_i}{\partial \alpha_2} & \dfrac{N_i}{R_2} & 0 & 0 \\ -\dfrac{N_i}{R_1} & 0 & \dfrac{1}{A}\dfrac{\partial N_i}{\partial \alpha_1} & 0 & 0 \\ 0 & -\dfrac{N_i}{R_2} & \dfrac{1}{B}\dfrac{\partial N_i}{\partial \alpha_2} & 0 & 0 \end{bmatrix}_{i=1,2,\ldots,9}, \tag{A.5}$$

$$[S] = \begin{bmatrix} N_{11} & N_{12} & 0 & 0 & 0 & 0 \\ N_{12} & N_{22} & 0 & 0 & 0 & 0 \\ 0 & 0 & N_{11} & N_{12} & 0 & 0 \\ 0 & 0 & N_{12} & N_{22} & 0 & 0 \\ 0 & 0 & 0 & 0 & N_{11} & N_{12} \\ 0 & 0 & 0 & 0 & N_{12} & N_{22} \end{bmatrix}, \tag{A.6}$$

where N_{ij} are the force resultants expressed in equation (8).